Geochemical Perspectives Letters

Microbial nitrogen cycle enhanced by continental input recorded in the Gunflint Formation

A. Ishida[1†*], K. Hashizume[2‡], T. Kakegawa[1]

OPEN ACCESS

doi: 10.7185/geochemlet.1729

Abstract

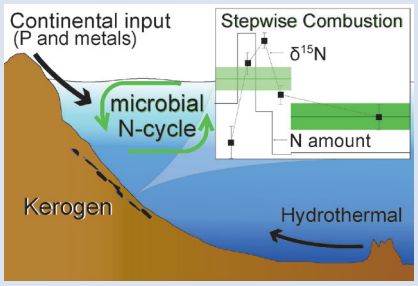

Nitrogen isotope compositions ($\delta^{15}N$ values) of kerogen in the sedimentary rocks from the 1878 Ma Gunflint Formation were analysed to understand the relationships among microbial activities, ocean chemistry, and tectonic evolution in the Animikie Basin. In the present study, the stepwise combustion analysis, performed on 13 kerogen samples, indicates that the $\delta^{15}N$ values of kerogen can be sub-divided into two fractions with discrete values depending on the combustion temperatures: a lower-temperature fraction (from 500 to 575 ˚C), and a higher-temperature fraction (higher than 575 ˚C). A positive correlation was observed between the $\delta^{15}N$ values of the lower-temperature fractions and Pr/Sm ratios, which represent contributions from the continental input. In contrast, no correlation was observed between the $\delta^{15}N$ values of the higher-temperature fractions and the Pr/Sm ratios. This relationship between the $\delta^{15}N$ values and the continental inputs is explained by the isotopic fractionation effects of the biological nitrogen cycle associated with the enhanced microbial activity, triggered by the active tectonic settings in the Animikie basin.

Received 17 February 2017 | Accepted 21 June 2017 | Published 5 August 2017

Introduction

The nitrogen isotope compositions ($\delta^{15}N$ values) of organic matter (OM) found in ancient sedimentary rocks are used as proxies for reconstructing the microbial nitrogen cycle and the palaeo-oceanic environment (*e.g.*, Beaumont and Robert, 1999, Shen *et al.*, 2006; Ader *et al.*, 2016; Stüeken *et al.*, 2016). OM in sedimentary rock is considered to be a complex mixture of several organisms, however, they are poorly understood. In the stepwise combustion method, components hosted by different carriers, which are intimately mixed in a sample and cannot be separated by other physical methods, can be resolved based on the combustion temperature. A preliminary study was performed using kerogen samples extracted from two rock samples from the Gunflint Formation, indicating temperature-dependent $\delta^{15}N$ heterogeneities within each kerogen sample (Ishida *et al.*, 2012). In this study, we further examined 11 samples in search of internal $\delta^{15}N$ heterogeneities in the Gunflint kerogen.

The Gunflint Formation, belonging to the Animikie Group, is located on the northwestern shore of Lake Superior, Ontario, Canada (Goodwin, 1956). The age of the Gunflint Formation is estimated as 1878 ± 1.3 Ma by U-Pb dating (Fralick *et al.*, 2002). An evolution model for the Animikie Basin has been proposed by, *e.g.*, Schulz and Cannon (2007). The tectonic evolution in this region leads to transition from foreland-type volcanism to the back-arc type volcanism, resulting in active supply of detrital material from the continent. In the present study, samples were collected covering the variation representative of shallow to deep lithology. Lithology and whole rock major and trace element geochemistry, which were consistent with previous studies, are summarised in Supplementary Information.

Stepwise Nitrogen Analysis of Kerogen

The stepwise combustion method discriminates organic nitrogen fractions with different chemical natures. The analytical protocols and performances are described in Ishida *et al.* (2012), and references therein. Kerogen samples were combusted in an oxygen atmosphere with temperatures from 450 °C to 1100 °C. No isotope measurement was performed at 450 °C, where surficial contamination, such as adsorbed nitrogen and/or ammonium ions, dominates. Empirically two distinct nitrogen isotope plateaus appear in kerogen analyses: one appears at temperatures between 475 °C and 575 °C (lower temperature fraction: LT-fraction), and the other appears at temperatures more than 575 °C (higher temperature fraction: HT-fraction) (Ishida *et al.*, 2012). Between 475 °C and 575 °C, combustion temperatures were increased in 25 °C steps to precisely resolve LT- and HT-fractions. Beyond this temperature range, one batch of combustion was performed at 1100 °C for analyses of the HT-fraction. Besides the stepwise combustion, $\delta^{15}N$ values of bulk kerogen were also determined.

1. Department of Earth Science, Graduate School of Science, Tohoku University, Sendai 980-8578, Japan
† Present address: Institute for Excellence in Higher Education, Tohoku University, Sendai 980-8576, Japan
* Corresponding author (email: ishidaz@m.tohoku.ac.jp)
2. Department of Earth and Space Sciences, Graduate School of Science, Osaka University, Toyonaka 560-0043, Japan
‡ Present address: Division of Earth and Environmental Science, Faculty of Science, Ibaraki University, Mito 3108512, Japan

Nitrogen Isotope Heterogeneity in Gunflint Kerogen

The $\delta^{15}N$ values of the bulk kerogen samples, ranging between +2.9 and +8.0 ‰, are consistent with previous reports (*e.g.*, Beaumont and Robert, 1999; Godfrey *et al.*, 2013). The isotope shift by metamorphism can induce preferential release of ^{14}N from the OM. However, the low metamorphic grade of the Gunflint Formation (below greenschist facies) cannot be responsible for a significant fractionation, up to 5 ‰ (*e.g.*, Haendal *et al.*, 1986, Ader *et al.*, 2016). The lack of systematic correlation between $\delta^{15}N$ values and C/N ratios among kerogen samples expected by the metamorphism (*e.g.*, Haendal *et al.*, 1986) supports the above argument (Fig. S-3).

The modern marine biosphere involves a nitrogen biological cycle that consists mainly of fixation ($N_2 \rightarrow NH_4^+$), nitrification ($NH_4^+ \rightarrow NO_2^- \rightarrow NO_3^-$), and denitrification ($NO_3^-$, $NO_2^- \rightarrow N_2$). When biological N_2 fixation is dominant, the $\delta^{15}N$ values of OM tend to be close to the atmospheric value (0 ‰), because of minimal isotopic fractionation expected in fixation. However, when nitrification and denitrification are coupled with fixation, the $\delta^{15}N$ value of OM may grow to positive values. This isotopic shift is considered as evidence of isotopic fractionation driven by biological nitrification and denitrification (*e.g.*, Shen *et al.*, 2006; Brandes *et al.*, 2007; Sigman *et al.*, 2009; Hashizume *et al.*, 2016). The $\delta^{15}N$ values of OM can vary depending on the balance between the rate of N_2 fixation and the rates of nitrification/denitrification (*e.g.*, Lehmann, *et al.*, 2002, Pinti and Hashizume, 2011). For example, Papineau *et al.* (2013) reported that the $\delta^{15}N$ values of OM in Palaeoproterozoic Indian sedimentary formations were approximately 0 ‰. These values were interpreted to be the result of a system dominated by N_2 fixation associated with cyanobacterial blooms. In contrast, our data show much more positive $\delta^{15}N$ values for the bulk kerogen samples, reaching values as high as +8 ‰. Such positive values suggest that nitrite and nitrate were available in the Gunflint ocean. Kerogen from Palaeoproterozoic samples, except for phosphatic shales, also exhibit positive values, up to +12 ‰ (*e.g.*, Beaumont and Robert, 1999; Papineau *et al.*, 2009, Godfrey *et al.*, 2013, Stüeken *et al.*, 2016). To operate such a biological nitrogen cycle, oxygenated surface water is required at this time.

Stepwise combustion analyses of $\delta^{15}N$ were performed on kerogen samples mainly from the Current River section (see Supplementary Information and Table S-2). In this section, the lithology changed from shale (#0714, #0715) to carbonate-sand zone (#0711 to #0703) to arkosic sandstone (#0701, #0702). Such lithological changes represent a local marine regression. Figure 1 shows the results of the stepwise combustion analyses performed on 13 kerogen samples in our study. The average $\delta^{15}N$ values of the LT-fractions and the HT-fractions ($\delta^{15}N_{LT}$ and $\delta^{15}N_{HT}$, respectively) were calculated using the $\delta^{15}N$ values and the released amounts for the relevant temperature steps. Some samples exhibited higher $\delta^{15}N_{HT}$ than $\delta^{15}N_{LT}$, while other samples exhibited the opposite trend. The ranges of the $\delta^{15}N$ values for both fractions are similar to the overall range of bulk kerogen $\delta^{15}N$ values. In most samples, the HT-fractions have lower amounts of nitrogen than those of the LT-fractions. The differences in the combustion temperature possibly correspond to differences in the carbon structure for fractions of kerogen that co-exist in OM (Ishida *et al.*, 2012).

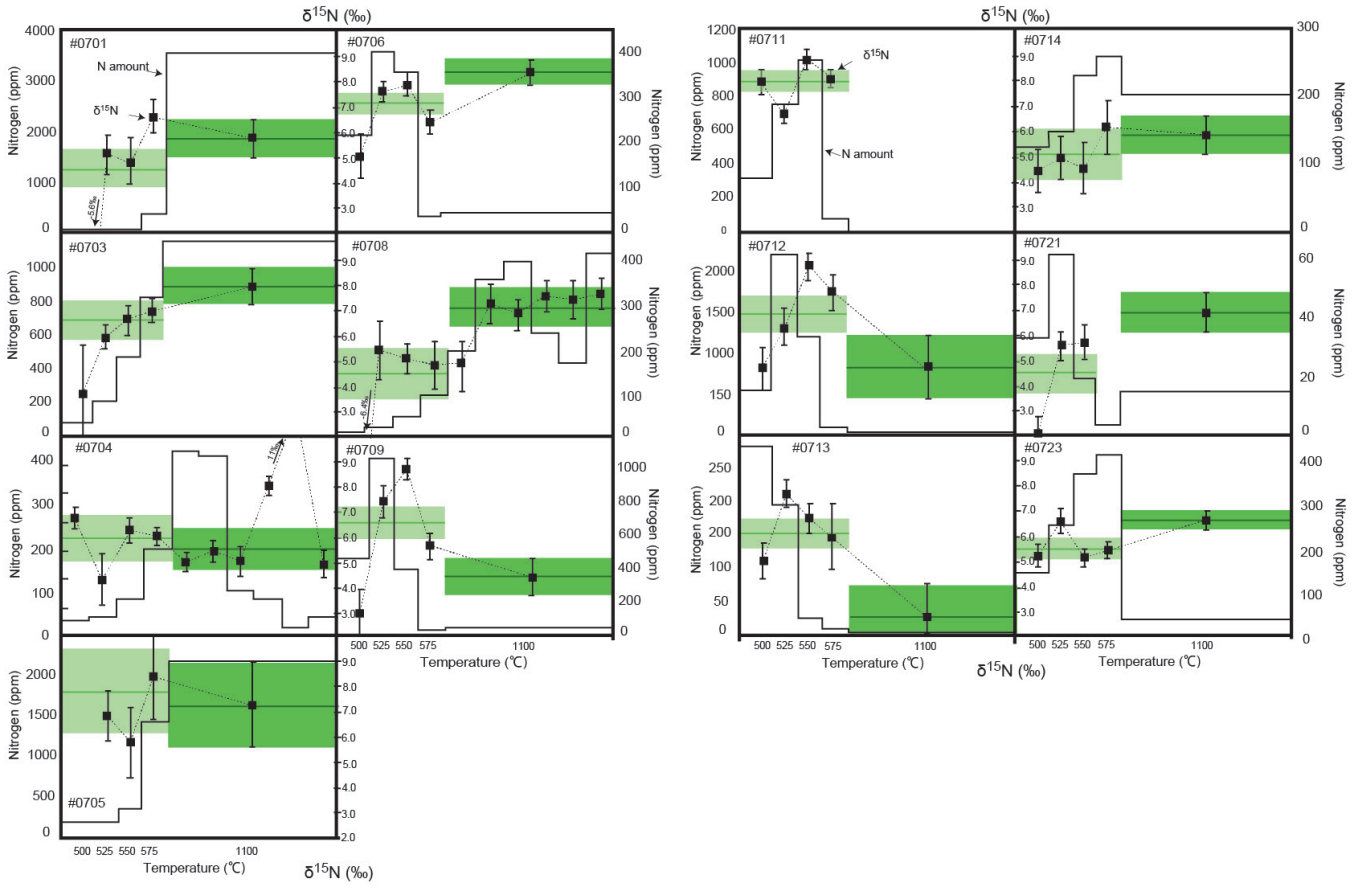

Figure 1 Results of the stepwise combustion analyses of 13 kerogen samples from the Gunflint Formation (samples #0704 and #0708 are cited from Ishida *et al.*, 2012). Nitrogen concentrations (white bars) and $\delta^{15}N$ values (black squares) are shown. The average $\delta^{15}N$ values and errors of both the lower-temperature and the higher-temperature fractions are shown as light green and dark green bars, respectively. Original data are summarised in Table S-2.

Table 1 Summary of light and trace element concentrations and the isotope compositions of bulk rock and kerogen samples.

section	sample ID	litho facies	bulk rock						kerogen								
			Total C	TOC	C_{carb}	S_{pyr}	Pr/Sm	Eu/Eu*	C	N	H	S	C/N	$\delta^{13}C$	$\delta^{34}S$ (pyr)	$\delta^{15}N$	±
			wt. %				(PAAS normalised)[1]		wt. %				atom	‰			
Pass Lake Road	0716	Chert	0.1	0.0	0.1	0.0	1.22	0.87	n.a.	n.a.	n.a.	n.a.	-	n.a.	n.a.	n.a.	n.a.
	0718	Carbonate	6.6	0.0	6.6	0.0	0.61	2.22	n.a.	n.a.	n.a.	n.a.	-	n.a.	n.a.	n.a.	n.a.
	0719	Silicified carbonate	3.1	0.0	3.1	0.0	0.66	2.24	n.a.	n.a.	n.a.	n.a.	-	n.a.	n.a.	n.a.	n.a.
	0720	Silicified carbonate	3.7	0.1	3.6	0.0	0.67	2.18	n.a.	n.a.	n.a.	n.a.	-	n.a.	n.a.	n.a.	n.a.
	0721	Taconite	3.0	0.2	2.9	0.6	0.82	1.78	16.8	0.2	0.3	32.6	109.6	-32.6	3.0	4.7	0.60
	0722	Chert (BIF)	0.2	0.0	0.2	0.0	0.88	1.73	n.a.	n.a.	n.a.	n.a.	-	n.a.	n.a.	6.8	1.00
	0723	Carbonate (BIF)	5.2	0.1	5.1	0.1	0.82	1.41	n.a.	n.a.	n.a.	n.a.	-	-25.1	n.a.	5.4	0.40
Blend River North	0301	Black shale	0.3	0.3	0.0	0.0	1.76	1.25	70.7	1.2	3.5	5.6	67.4	-31.6	2.1	2.9	0.70
	0302	Black shale	0.8	0.3	0.5	0.2	0.49	1.48	53.1	0.6	2.4	18.2	96.2	-31.6	4.7	n.a.	n.a.
	0303	Ferruginous shale	4.1	0.3	3.8	0.1	0.76	1.54	69.4	1.2	3.2	9.6	67.6	-31.3	7.1	n.a.	n.a.
	0304	Black shale	1.1	0.9	0.1	0.0	1.43	1.19	73.1	1.1	3.2	3.2	75.5	-32.1	8.6	5.9	0.70
	0305	Carbonate	9.1	0.8	8.3	0.4	0.69	1.59	49.8	0.9	2.0	18.8	64.7	-31.9	8.2	6.5	0.70
	0306	Ferruginous carbonate	10.4	0.3	10.2	0.1	0.78	1.32	60.5	1.1	2.9	13.3	63.9	-29.8	n.a.	n.a.	n.a.
	0307	Silicified carbonate	5.0	0.1	4.9	0.0	0.78	1.54	n.a.	n.a.	n.a.	n.a.	-	n.a.	n.a.	n.a.	n.a.
	0308	Carbonate/shale	4.0	0.0	3.9	0.0	0.83	1.18	44.1	0.0	0.0	15.2	-	n.a.	n.a.	n.a.	n.a.
	0309	Ferruginous carbonate	9.9	0.2	9.7	0.0	0.83	1.27	76.0	1.4	3.5	5.7	65.6	n.a.	n.a.	n.a.	n.a.
	0310	Chert	3.2	0.1	3.1	0.0	0.83	1.29	n.a.	n.a.	n.a.	n.a.	-	n.a.	n.a.	n.a.	n.a.
	0311	Chert	1.9	0.0	1.8	0.0	0.68	0.72	60.3	0.7	2.2	8.5	94.9	n.a.	n.a.	n.a.	n.a.
Current River	0701	Carbonate-rich arkosic sandstone	4.7	0.5	4.2	0.0	0.86	1.28	67.3	0.9	2.2	5.6	91.2	-33.0	26.9	5.6	0.80
	0702	Arkosic sandstone	0.8	0.2	0.6	0.0	1.87	1.11	56.6	0.6	3.2	2.5	101.7	-32.2	8.3	6.7	0.70
	0703	Sandy carbonate	4.2	0.2	4.0	0.0	0.99	1.24	82.7	1.1	3.7	2.8	88.5	-32.3	10.9	7.1	0.50
	0704	Sandy carbonate	5.9	0.2	5.7	0.0	0.98	1.18	82.9	1.0	3.8	3.2	98.4	-32.5	11.2	4.9	1.00
	0705	Sandy carbonate	4.4	0.1	4.3	0.0	1.23	1.42	52.6	0.7	2.2	14.8	86.8	-31.6	9.7	6.0	0.70
	0706	Sandy carbonate	5.4	0.3	5.1	0.2	1.03	1.52	47.8	0.6	2.0	19.6	87.6	-32.6	15.1	6.9	0.60
	0707	Sandy carbonate	2.9	0.2	2.8	0.0	0.92	1.18	66.1	0.8	2.8	10.2	98.3	-31.9	5.8	5.9	0.80
	0708	Sandy carbonate	7.1	0.3	6.7	0.0	0.76	1.76	85.7	1.0	4.1	1.6	98.8	-32.9	16.0	6.9	0.50
	0709	Laminated carbonate with detrital quartz	1.8	0.2	1.6	0.1	1.03	1.31	59.9	0.8	2.5	14.2	86.7	-32.4	14.8	7.3	0.60
	0710	Laminated carbonate with detrital quartz	0.3	0.1	0.2	0.0	1.18	1.48	72.1	1.0	4.4	5.9	80.3	-32.0	-	3.2	0.60
	0711	Massive carbonate	9.0	0.1	8.9	0.1	0.93	1.63	54.3	0.8	2.9	14.6	80.9	-32.6	13.4	8.0	0.40
	0712	Laminated carbonate with detrital quartz	0.7	0.3	0.4	0.1	1.16	1.63	66.0	1.0	3.4	9.4	78.3	-32.5	11.3	7.2	0.30
	0713	Carbonate shale (phosphorous)	6.2	0.2	6.0	0.1	1.02	1.68	43.2	0.6	1.8	20.7	90.1	-32.4	9.2	6.4	0.60
	0714	Black shale	4.5	0.9	3.7	0.1	1.42	1.22	68.6	1.0	3.0	4.8	78.2	-33.6	9.3	4.8	0.90
	0715	Black shale	0.2	0.3	0.0	0.0	1.20	1.28	8.2	0.2	1.2	1.6	61.3	-32.2	11.5	5.9	0.70
Telly Fox	0724	Carbonate	9.7	0.3	9.3	0.2	0.93	1.53	37.8	0.6	1.7	25.4	77.5	-31.4	-1.1	n.a.	n.a.
	0725	Silicified shale	0.2	0.2	0.0	0.4	0.63	1.23	n.a.	n.a.	n.a.	n.a.	-	-31.5	20.7	5.5	0.70
	0726	Carbonate/shale	0.3	0.4	0.0	0.2	0.71	1.40	60.1	0.9	2.9	12.5	78.6	-31.6	10.8	4.5	0.30
	0729	Silicified carbonate	0.3	0.1	0.3	0.1	0.24	0.72	n.a.	n.a.	n.a.	n.a.	-	-28.9	n.a.	4.3	0.30
	0730	Silicified carbonate	0.3	0.1	0.2	0.0	0.20	0.99	n.a.	n.a.	n.a.	n.a.	-	n.a.	n.a.	n.a.	n.a.
Kaka-beka Fall	0601	Shale (BIF)	7.3	0.8	6.6	0.2	0.92	1.67	64.8	1.2	2.8	9.9	62.5	-31.3	5.9	6.3	0.80
	0602	Chert (BIF)	0.3	0.1	0.2	0.0	0.41	0.87	57.5	1.0	2.5	8.5	68.2	-29.7	n.a.	n.a.	n.a.
	0603	Shale (BIF)	5.5	0.4	5.1	0.1	0.84	1.46	60.6	1.0	2.0	12.2	70.8	-30.9	6.1	n.a.	n.a.
	0604	Ferruginous chert	2.7	0.1	2.6	0.1	1.16	1.37	46.4	0.9	1.6	15.6	60.3	-27.8	n.a.	n.a.	n.a.
	0605	Ferruginous chert	0.0	0.0	0.0	0.0	0.75	0.72	n.a.	n.a.	n.a.	n.a.	-	n.a.	n.a.	n.a.	n.a.

Analytical error of $\delta^{13}C$ and $\delta^{34}S$ are within 0.2 ‰.
Underlined values: below instumental reproducibility (0.1 %). n.a.: not analysed because of low amount of organic matter.
[1] Details are described in Tables S-1 and S-4.

The nitrogen released in the HT-fraction possibly has stronger bonds with carbon in the form of graphitised kerogen, compared to the LT-fraction. Ishida *et al.* (2012) concluded that the HT-fraction might not be a metamorphosed portion of OM with the same origin as the LT-fraction, since the HT-fraction does not always show higher $\delta^{15}N$ values than the LT-fraction. Because the chemical structures of kerogen are known to be heterogeneous, some components of kerogen are easy to graphitise but the others are non-graphitised (*e.g.*, Bustin *et al.*, 1995; Beyssac *et al.*, 2002). We interpret the OM observed in the HT-fraction to represent the residue of graphitised parts of kerogen. Such graphitisation could be promoted by the heterotrophic microbial degradation during diagenesis. Thus, we interpret the nitrogen in the LT-fractions to represent more indigenous nitrogen isotope compositions in the ecosystem at that time.

A positive correlation was observed between the $\delta^{15}N_{LT}$ and the Pr/Sm ratios of bulk rock (Fig. 2a). The Pr/Sm ratios among our samples are interpreted to represent the contribution of continental inputs to the ocean, supported by the negative correlation with Eu/Eu* (Bolhar *et al.*, 2005) (Fig. 3a), and positive correlations with abundances of elements that represent detrital inputs (Fig. 3b,c). The $\delta^{15}N_{HT}$ showed a poor correlation with the Pr/Sm ratios (Fig. 2b). The variable $\delta^{15}N_{LT}$ values in a positive range and their correlation to the Pr/Sm ratios could be caused by intense nitrification/denitrification when the nutrient supply from the land enhanced.

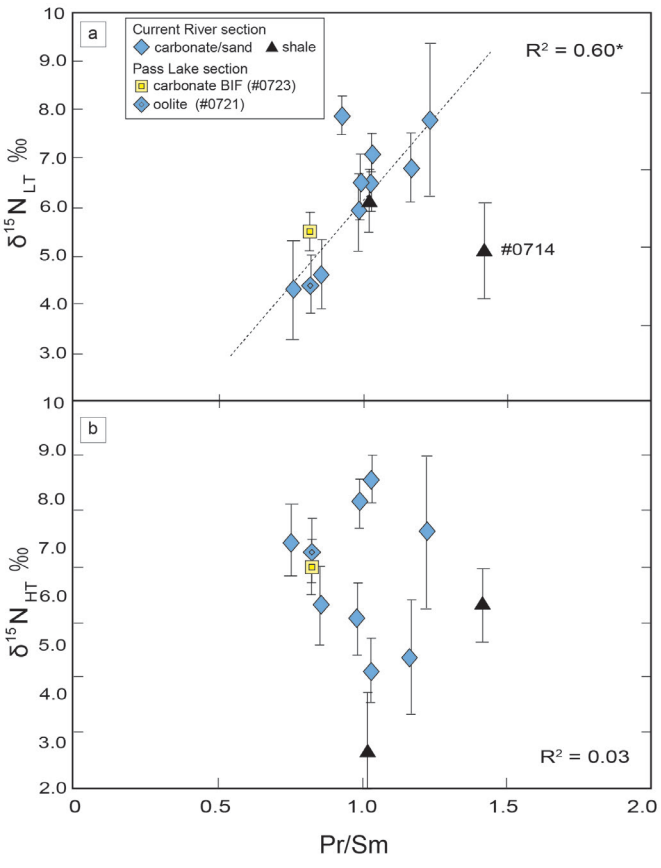

Figure 2 Correlation diagrams between the Pr/Sm ratios and **(a)** the $\delta^{15}N_{LT}$ values and **(b)** the $\delta^{15}N_{HT}$ values, respectively. A positive correlation is observed between the Pr/Sm ratios and the $\delta^{15}N_{LT}$ values ($R^2 = 0.60$, excluding #0714), whereas no correlation is observed between the $\delta^{15}N_{HT}$ values.

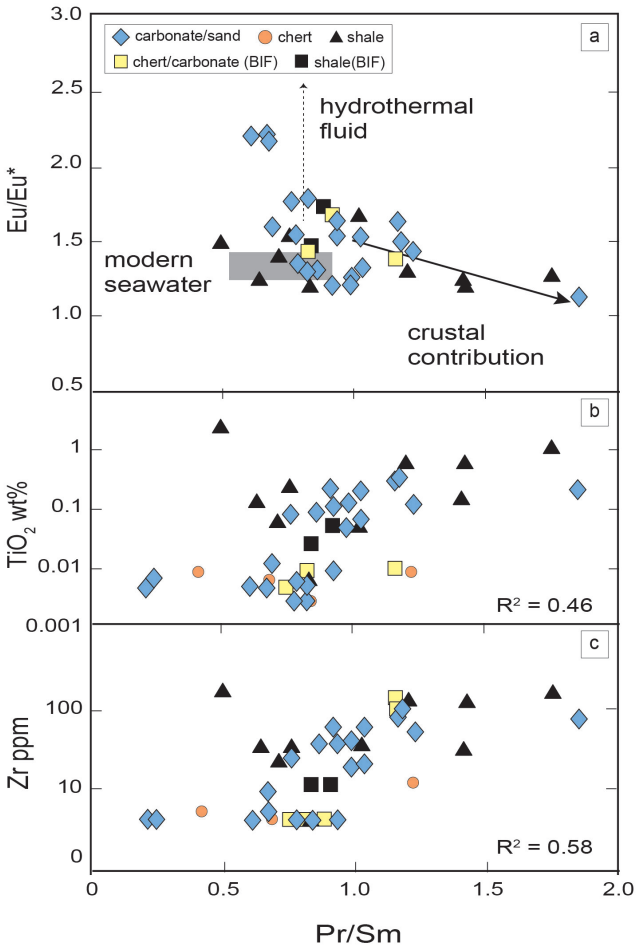

Figure 3 Correlation diagrams between the Pr/Sm ratios and **(a)** the Eu/Eu* ratios, **(b)** TiO_2, and **(c)** Zr concentrations. The Eu/Eu* is defined as Eu/0.5(Gd+Sm). Grey square areas indicate the range of modern ocean values. Dashed and solid arrows indicate the directions of hydrothermal fluid and crustal contributions, respectively (Bolhar *et al.*, 2005). Positive correlations exist between the Pr/Sm and TiO_2 and Zr concentrations.

Palaeo-ecosystem in the Gunflint Ocean

The carbon isotope compositions ($\delta^{13}C$ values) of the examined kerogen samples, ranging from -33.6 to -25.1 ‰, are consistent with the carbon isotope values fixed by cyanobacteria (*e.g.*, Schidlowski, 1988; House *et al.*, 2000). The $\delta^{13}C$ of kerogen in the sedimentary rocks, in general, corresponds to the values of contemporary primary producers. The presence of oxygenic primary producers in the Gunflint ocean is consistent with the biological nitrogen cycle proposed in the present study, and with the mineralogical and trace element geochemistry (see Supplementary Information).

The OM sinking through the water column would consume the dissolved oxygen, producing a temporary or partial sub-oxic zone in the Gunflint ocean, similar to a red tide event in the modern ocean (Minagawa and Wada, 1986). In the water column with spatially variable redox conditions ranging from oxic to anoxic, nitrification/denitrification processes could be enhanced, thereby inducing ^{15}N enrichment in the OM (*e.g.*, Shen *et al.*, 2006; Sigman *et al.*, 2009). One of the triggers of red tide in the modern ocean environment is considered to be an increased amount of nutrient supply to the ocean from the land (*e.g.*, Taylor *et al.*, 1995; Valiela *et al.*, 1997; Hauxwell *et al.*, 1998). The rapid growth of continents in the Animikie basin enhanced the supply of elements from

the terrestrial region to the Gunflint ocean. Our data suggest that increased continental input brought more phosphorus and trace metal elements to the sedimentary environment (Fig. S-3, Table S-5), rather than modern-like nutrients such as dissolved OM, which are less likely at this time. The increased flux of such elements into the Gunflint ocean would promote the high production and nitrogen cycling in the biosphere of the shallow ocean (*e.g.*, Papineau *et al.*, 2009; Edwards *et al.*, 2012; Stüeken *et al.*, 2015), as represented by the positive correlation between Pr/Sm ratios and $\delta^{15}N_{LT}$ of kerogen observed in this study.

The active production of OM may have facilitated the formation of the organic-rich sediments as well. The high flux of OM would keep the interior of sediments under suboxic to anoxic conditions, where the activity of sulphate-reducing bacteria was promoted. Such conditions would produce the heavier $\delta^{34}S$ values in the final products, such as pyrite (see Table 1 and Supplementary Information). A local involvement of methanogens and methanotrophs in such a benthic or subsurface environment is also plausible and is supported by the carbon isotope study of microfossils (House *et al.*, 2000). The primary OM precipitated to the sea floor would be decomposed by those heterotrophic bacteria, resulting in nitrogen isotope heterogeneities in the kerogen left in the sediments. The combined approaches of stepwise nitrogen isotope analyses and multiple geochemical analyses in this study can be used as a proxy to understand the evolution of biosphere and ocean environment in the Precambrian age.

Acknowledgements

Constructive reviews by Dr. Stüeken and an anonymous reviewer greatly helped to improve the quality of the article. This research was supported by Grant-in-Aid for JSPS (DC1) to A.I. (21-2645), and by KAKENHI to T.K. (24403013, 15H021440), and K.H. (JP17340168).

Editor: Bruce Watson

Additional Information

Supplementary Information accompanies this letter at www.geochemicalperspectivesletters.org/article1729

Reprints and permission information are available online at http://www. geochemicalperspectivesletters.org/copyright-and-permissions

Cite this letter as: Ishida, A., Hashizume, K., Kakegawa, T. (2017) Microbial nitrogen cycle enhanced by continental input recorded in the Gunflint Formation. *Geochem. Persp. Let.* 4, 13–18.

References

Ader, M., Thomazo, C., Sansjofre, P., Busigny, V., Papineau, D., Laffont, R., Cartigny P., Halverson, G.P. (2016) Interpretation of the nitrogen isotopic composition of Precambrian sedimentary rocks: assumptions and perspectives. *Chemical Geology* 429, 93–10.

Beaumont, V., Robert, F. (1999) Nitrogen isotope ratios of kerogens in Precambrian cherts: a record of the evolution of atmosphere chemistry? *Precambrian Research* 96, 63–82.

Beyssac, O., Rouzaud, J.N., Goffe', B., Brunet, F., Chopin, C. (2002) Graphitization in a high-pressure, low-temperature metamorphic gradient: a Raman microspectroscopy and HRTEM study. *Contributions to Mineralogy and Petrology* 143, 19–31.

Bolhar, R., Van Krenendonk, M., Kamber, B.S. (2005) A trace element study of siderite-jasper banded iron formation in the 3.45 Ga Warrawoona Group, Pilbara Craton-Formation from hydrothermal fluids and shallow seawater. *Precambrian Research* 137, 93–114.

Brandes, J.A., Devol, A.H., Deutsch, C. (2007) New Developments in the Marine Nitrogen Cycle. *Chemical Reviews* 107, 577–589.

Bustin, R.M., Ross, J.V. Rouzaud, J.N. (1995) Mechanisms of graphite formation from kerogen: Experimental evidence. *International Journal of Coal Geology* 28, 1–36.

Edwards, C.T., Pufahl, P.K., Hiatt, E.E., Kyser, T.K. (2012) Paleoenvironmental and taphonomic controls on the occurrence of Paleoproterozoic microbial communities in the 1.88 Ga Ferriman Group, Labrador Trough, Canada. *Precambrian Research* 212–213, 91–106.

Fralick, P., Davis, D.W., Kissin, S.A. (2002) The age of Gunflint Formation, Ontario, Canada: single zircon U-Pb age determinations from reworked volcanic ash. *Canadian Journal of Earth Science* 39, 1085–1091.

Godfrey, L.V., Poulton, S.W., Bebout, G.E., Fralick, P.W. (2013) Stability of the nitrogen cycle during development of sulfidic water in the redox-stratified late Paleoproterozoic Ocean. *Geology* 41, 655–658.

Goodwin, A.M. (1956) Facies relations in the Gunflint iron formation. *Economic Geology* 51, 565-595.

Haendal, D., Muhle, K., Nitzsche, H., Stiehl, G., Wand, U. (1986) Isotopic variations of the fixed nitrogen in metamorphic rocks. *Geochimica et Cosmochimica Acta* 50, 749–758.

Hashizume, K., Pinti, D.L., Orberger, B., Cloquet, C., Jayananda, M., Soyama, H. (2016) A biological switch at the ocean surface as a cause of laminations in a Precambrian iron formation. *Earth Planetary Science Letters* 446, 27–36.

Hauxwell, J., McClelland, J., Behr, P.J., Valiela, I. (1998) Relative importance of grazing and nutrient controls of macroalgal biomass in three temperate shallow estuaries. *Estuaries* 21, 347–360.

House, H.C., Schopf, J.W., McKeegan, K.D., Coath, C.D., Harrison, T.M., Stetter, K.O. (2000) Carbon isotopic composition of individual Precambrian microossils. *Geology* 28, 707–710.

Ishida, A., Hashizume, K., Kakegawa, T. (2012) Stepwise combustion analyses of distinct nitrogen isotopic compositions on Paleoproterozoic organic matter, *Geochemical Journal* 46, 249–253.

Lehmann, M.R., Bemasconi, S.M., Barbieri, A., McKenzie, J.A. (2002) Preservation of organic matter and alteration of its carbon and nitrogen isotope composition during simulated and in situ early sedimentary diagenesis. *Geochimica et Cosmochimica Acta* 66, 3573–3584.

Minagawa, M., Wada, E. (1986) Nitrogen isotope ratios of red tide organisms in the east china sea: A characterization of biological nitrogen fixation. *Marine Chemistry* 19, 245–259.

Papineau, D., Purohit, R., Goldberg, T., Pi, D., Shields, G.A., Bhu, H., Steele, A., Fogel, M.L. (2009) High primary productivity and nitrogen cycling after the Paleoproterozoic phosphogenic event in the Aravalli Supergroup, India. *Precambrian Research* 171, 37–56.

Papineau, D., Purohit, R., Fogel, M.L., Shields-Zuo, G.A. (2013) High phosphate availability as a possible cause for massive cyanobacterial production of oxygen in the Paleoproterozoic atmosphere. *Earth and Planetary Science Letters* 362, 225–236.

Pinti, D.L., Hashizume, K. (2011) Early life record from nitrogen isotopes. In: Golding, S., Glikson, M. (Eds.) *Earliest Life on Earth: Habitats, Environments and Methods of Detection*. Springer, Netherlands, 183–205.

Schidlowski, M. (1988) A 3,800-million-year isotopic record of life from carbon in sedimentary rocks. *Nature* 333, 313–318.

Schulz, K.J., Cannon, W.F. (2007) The Penokean orogeny in the Lake Superior region. *Precambrian Research* 157, 4–25.

Shen, Y., Pinti, D.L., Hashizume, K. (2006) Biogeochemical cycles of sulfur and nitrogen in the Archean ocean and atmosphere. In: Benn, K., Mareschal, J.C., Condie, K. (Eds.) *Archean Geodynamics and Environments, Geophyscal Monograph Series* 164, 305–320.

Sigman, D.M., Karsh, K.L., Casciotti, K.L. (2009) Ocean process tracers: nitrogen isotopes in the ocean. In: Steele, J.H., Thorpe, S.A., Turekian, K.K. (Eds.) *Encyclopedia of Ocean Science*. Elsevier, Amsterdam, 4138–4153.

Stüeken, E.E., Buick, R., Guy, B.M., Koehler, M.C. (2015) Isotopic evidence for biological nitrogen fixation by molybdenum-nitrogenase from 3.2 Gyr. *Nature* 520, 666–674.

Stüeken, E.E., Kipp, M.A., Koehler, M.C., Buick, R. (2016) The evolution of Earth's biogeochemical nitrogen cycle. *Earth-Science Reviews* 160, 220–239.

Taylor, D., Nixon, S., Granger, S., Buckley, B. (1995) Nutrient limitation and the eutrophication of coastal lagoons. *Marine Ecology Progress Series* 127, 235–244.

Valiela, I., McClelland, J., Hauxwell, J., Behr, P.J., Hersh, D., Foreman, K. (1997) Macroalgal blooms in shallow estuaries: Controls and ecophysiological and ecosystem consequences. *Limnology and Oceanography* 42, 1105–1118.